Phonon spectra of strongly luminescent non-stoichiometric Ag-In-S, Cu-In-S, and Hg-In-S nanocrystals of small size

Volodymyr Dzhagan[1,2,], Oleksandr Selyshchev[3], Oleksandra Raievska[3,4,5], Oleksandr Stroyuk[5,6], Lukas Hertling[3], Nazar Mazur[1], Mykhailo Ya. Valakh[1], Dietrich R.T. Zahn[3,4]*

[1] V. Lashkaryov Institute of Semiconductors Physics, National Academy of Sciences of Ukraine, Kyiv, Ukraine

[2] Taras Shevchenko National University of Kyiv, 64 Volodymyrs'ka St., 01601 Kyiv, Ukraine

[3] Semiconductor Physics, Chemnitz University of Technology, D-09107 Chemnitz, Germany

[4] Center for Materials, Architectures, and Integration of Nanomembranes (MAIN), Chemnitz University of Technology, D-09107 Chemnitz, Germany

[5] L.V. Pysarzhevsky Institute of Physical Chemistry, Nat. Acad. of Science of Ukraine, 03028 Kyiv, Ukraine.

[6] Forschungszentrum Jülich GmbH, Helmholtz-Institut Erlangen Nürnberg für Erneuerbare Energien (HI ERN), Immerwahrstr. 2, 91058 Erlangen, Germany

KEYWORDS $AgInS_2$, $CuInS_2$, $AgIn_5S_8$, $CuIn_5S_8$, chalcopyrite, spinel, Raman spectra, infrared absorption

ABSTRACT We present a detailed analysis of Raman and infrared (IR) phonon spectra of strongly luminescent non-stoichiometric M-In-S (M = Cu, Ag, Hg) and core/shell M-In-S/ZnS nanocrystals (NCs) of small size ($d \approx$ 2-4 nm), formed by means of aqueous colloidal chemistry under mild conditions. Despite presumably similar factors determining position and broadening of the Raman and X-ray diffraction (XRD) peaks, phonon spectra are shown to be more sensitive to NC composition and crystals structure. The spectral Raman pattern of these strongly M-deficient M-In-S NCs is different from that of the corresponding stoichiometric phases, *e.g.* $CuInS_2$ or $AgIn_5S_8$, and excludes its assignment to relevant binary sulfides, *e.g.* In_2S_3. Resonant behavior of relative peak intensities in Raman spectra is different from that of larger-size stoichiometric NCs and bulk samples studied before, while the temperature dependence reveals an analogous enhancement of the highest-frequency LO modes supporting an unambiguous assignment of the latter. Therefore, we conclude that the Raman spectra observed are characteristic of the specific structure of these highly non-stoichiometric small NCs. IR modes of these NCs occur in the same frequency range as the Raman ones but at higher frequencies than the IR phonons in bulk material. The IR spectra are less characteristic, compared to Raman ones, revealing more similarity among the three NC compounds and with the bulk counterparts.

Introduction

Colloidal I-III-VI nanocrystals (NCs) comprise one of the most promising types of metal-chalcogenides that have emerged in the recent years as a viable alternative to CdX and PbX (X = S, Se, Te) NCs [1–7]. Particularly interesting, both for fundamental studies and practical applications, are small (below 5 nm) M-In-S and core/shell M-In-S/ZnS (M = Ag, Cu, Hg) NCs, possessing untypically strong broad-band photoluminescence (PL), with quantum yields up to 95 % in non-polar solvents [8] and up to 60 % in water [5,6,9]. The nature of this PL is the subject of intense discussion in the literature [7,10–13] and may reflect some peculiarities of their electronic and lattice structure as well as electron-phonon coupling (EPC). A combination of the small size and tolerance towards strong non-stoichiometry can be the key to emerging new features in the electronic structure and optical properties, not existing in bulk crystals and larger (5-10 nm) stoichiometric NCs. The model based on radiative recombination of charges deeply trapped at donor and acceptor levels [14], which is most often used for explaining the large Stokes shift and full width at half maximum (FWHM) of these NCs, is unable to explain the PL dependence on temperature, NC size, and stoichiometry [5,6,9–11], as well as single NC PL results [15]. Recently, the large band width and Stokes shift, as well as temperature dependence of the highly efficient PL emission of Ag-In-S and similar ternary compound NCs was proposed to originate from a kind of self-trapped exciton (STE) state involving strong EPC [9]-[11]. Indications of a very strong contribution of optical phonons to PL, with up to nanosecond long lifetime, were indeed observed earlier for bulk $CuInS_2$ [16]. Therefore, knowing the phonon spectra of small M-In-S NCs is of crucial importance for understanding their EPC and optical properties. The high PL intensity can be a reason for the absence of thorough Raman studies of their phonons so far.

Besides providing the phonon spectra themselves, Raman spectroscopy is an efficient tool of probing both the lattice structure of semiconductor NCs and local resonances. Such resonances can be related either with intentional heterogeneity, like in core/shell structures [17–24] , or spontaneous formation of secondary phases and other kinds of structural inhomogeneity in complex chalcogenide NCs [25–32], which are not detectable by other structural techniques. These capabilities of Raman spectroscopy are based on spectrally well separated vibrational peaks related to different compounds, the possibility to selectively probe compounds/phases with different bandgaps by using resonant energy/wavelengths of the exciting light, and no special treatment of the sample needed for investigations. Being sensitive to the ionicity of bonds, the phonon frequencies may provide unique information about chemical bonds in a complex compound, also not accessible by other methods. A valuable complementary technique to Raman spectroscopy is far infrared (FIR) absorption, which allows Raman-inactive phonons to be probed. IR phonon spectra of M-In-S NCs have not been studied so far.

Here we report the Raman and IR phonon spectra of strongly luminescent (quantum yield up to 60 %) M-In-S and M-In-S/ZnS NCs of small size ($d \approx 3$ nm), formed by means of aqueous colloidal chemistry under mild conditions, and perform a detailed analysis of the spectra, including critically reviewed data from the literature and a support from own DFT calculations.

Experimental

The details about the aqueous synthesis and characterization of the NCs investigated in this work by PL, wide-angle X-ray diffraction (XRD), X-ray photoelectron spectroscopy (XPS), atomic force (AFM) and transmission electron (TEM) microscopy was already reported by us earlier [5,6,9,11,17]. For this study M-In-S NCs of average size about 3 nm were used, stabilized with glutathione. The UV-vis and PL (Fig. S1), XRD (Fig. S2), and XPS (Fig. S3) data are presented in the Supplementary Information. The possibility to measure Raman scattering on these highly luminescent NC samples was provided by adding a strong electron acceptor, methyl viologen dichloride (MV^{2+}) [33], that quenches PL strongly enough to acquire good quality Raman spectra. For acquiring Raman spectra, MV^{2+}-containing NC solutions were drop-casted on Si substrates and dried under ambient conditions. The samples for IR measurements were prepared by spin-coating of pristine NC solutions (without MV^{2+}) on gold mirror substrates.

Raman spectra were excited with a (λ_{exc} =) 488 nm DPSS laser (Sapphire, Coherent), 514.7 nm DPSS laser (Cobolt), 633 nm He-Ne laser or 325 nm He-Cd laser and registered with a LabRam HR spectrometer with a spectral resolution of 3 cm^{-1} for visible λ_{exc}'s and 5 cm^{-1} for 325 nm excitation. Raman spectra at λ_{exc} = 785 nm (DPSS laser) were registered using a Xplora Raman microscope (Horiba). The peak positions were determined with an accuracy better than 1 cm^{-1}. The incident laser power was kept below 0.1 mW (≈10 W/cm^2) in order to avoid sample heating under the microscope objective (50× for visible excitations and 40× for 325 nm). Low-temperature (80 K) Raman measurements were performed using a Linkam Stage THMS-600 micro-chamber. IR phonon spectra were collected in specular reflection geometry at an angle of 45° or in attenuation total reflection configuration (ATR) with a diamond crystal using a vacuum VERTEX 80v FTIR spectrometer (Bruker) equipped with a RT-DLaTGS detector and Mylar multilayer beam splitter. Density Functional Theory (DFT) calculations were performed with PWscf and PHonon Packages of the QUANTUM ESPRESSO software [34] [35]. The Dynmat code was used for the calculation of IR intensities and LO-TO splitting. The initial tetragonal $AgInS_2$ crystal structure was taken from the Crystallography Open Database [36].

Results and discussion

The most important feature of the luminescent NCs investigated in this work is, besides their small size, a strong deviation from the compositional stoichiometry of established bulk counterparts such as $CuInS_2$ and $AgIn_5S_8$. It was already shown in our previous studies, that for such I-III-VI NCs, synthesized in water using small thiol molecules as stabilizers, the highest PL efficiency is achieved not at a Cu:In (Ag:In) ratio of 1:1 but rather at highly Cu- or Ag-deficient compositions (like Cu:In or Ag:In molar ratios of 1:5 - 1:3) [5,6,9,11]. Similar trends were reported by other groups [1],[2] . The nominal M:In ratio set during the synthesis of the NCs studied in the present work was about 1:4, resulting in a real ratio in the NCs of about 1:3, according to the XPS data (Table 1 and Fig. S3,a). The net metal-to-Sulfur ratio is 40:60 for all compounds when both S^{2-} (lattice) and S^{1-} (shared lattice and ligand sulfur) species are taken into account (see SI, Fig. S3,b). When only S^{2-} is considered, the latter ratio becomes S-deficient for all three M-In-S compounds with respect to any of their tentative (bulk) modifications ($CuInS_2$, $AgIn_5S_8$, *etc.*). This fact is fully understood in view of the very

small NC size (2-4 nm) and stabilization mechanism by thiol ligands. Here, the Sulphur atom of the ligand, attached to the surface metal atoms of the NC (identified as S^{1-} in XPS spectra), is simultaneously a part of the NC lattice. Therefore, omitting this contribution in the calculation of the NC composition would result in (incorrectly) S-deficient compositions.

Table 1. XPS data on elemental ratios in the NCs studied.

AIS	**CIS**	**HIS**
Ag:In:S=12:29:59 Ag:In=28:72	Cu:In:S=9:30:61 Cu:In=23:77	Hg:In:S=10:28:62 Hg:In=26:74
AIS/ZnS	**CIS/ZnS**	**HIS/ZnS**
Ag:In:S:Zn=4:11:60:25 Ag:In=26:74 Ag:In:Zn=10:28:62 (Ag+In+Zn):S^{all}=41:59 (Ag+In+Zn):S^{2-}=78:22	Cu:In:S:Zn=2:13:61:24 Cu:In=15:85 Cu:In:Zn=6:33:61 (Cu+In+Zn):S^{all}=49:61 (Cu+In+Zn):S^{2-}=52:48	Hg:In:S:Zn=4:12:59:25 Hg:In=27:73 Hg:In:Zn=11:29:60 (Hg+In+Zn):S^{all}=41:59 (Hg+In+Zn):S^{2-}=55:45

Several features of the obtained elemental compositions have to be noted, which are of primary importance for the subsequent discussion/understanding of the phonon spectra. The ratio of M:In ≈ 1:3 can correspond either to a highly M-deficient M-In-S compound or to a 1:1 mixture of $MInS_2$ and MIn_5S_8. Therefore, in the following analysis and discussion of the phonon spectra and analysis of XRD patterns we have to consider this option at least for M = Ag, Cu ($HgIn_5S_8$ was not reported yet). They should also contribute to XRD patterns but are not discernable due to proximity of the corresponding reflexes (in bulk crystals) and substantial broadening of peaks in NCs. Another important observation from the XPS data is that the cation-anion ratio (~40:60) is not affected by adding Zn in all three compounds. This can mean that Zn does not take vacancies or substitutes other cations but extends the lattice (template) given by the M-In-S core NC. Even more interesting is a reduced Cu/In ratio in the core/shell NCs, while Ag/In and Hg/In ratios are not affected. Possible reasons will be discussed in the section devoted to phonons in core/shell NCs.

Figure 1 shows representative room-temperature (RT) phonon Raman spectra of Ag-In-S NCs at different λ_{exc}. The sharp peak at 520 cm^{-1} comes from Si substrate [37],

while weaker peaks at 686 and 822 cm^{-1} are due to vibrations of methyl viologen (MV) [38]. As the relative contribution of the lower-frequency MV peaks gets progressively enhanced towards longer λ_{exc} (Fig. 1a), MV mode at about 280 cm^{-1} needs to be taken into account when analyzing the NC phonon spectra measured with λ_{exc}=633 nm. In order to confirm the origin of the latter mode from MV, as well as its relative intensity, we investigated composites of MV with similarly synthesized aqueous NCs of other compounds (*e.g.* CdTe), which do not have phonon features around 280 cm^{-1} (Fig. S4). Due to the negligible contribution of the latter MV mode to the NC spectra at 488 nm, spectra taken at this λ_{exc} are mostly used in the following analysis of vibrations in Ag-In-S, Cu-In-S, and Hg-In-S NCs (Fig. 2).

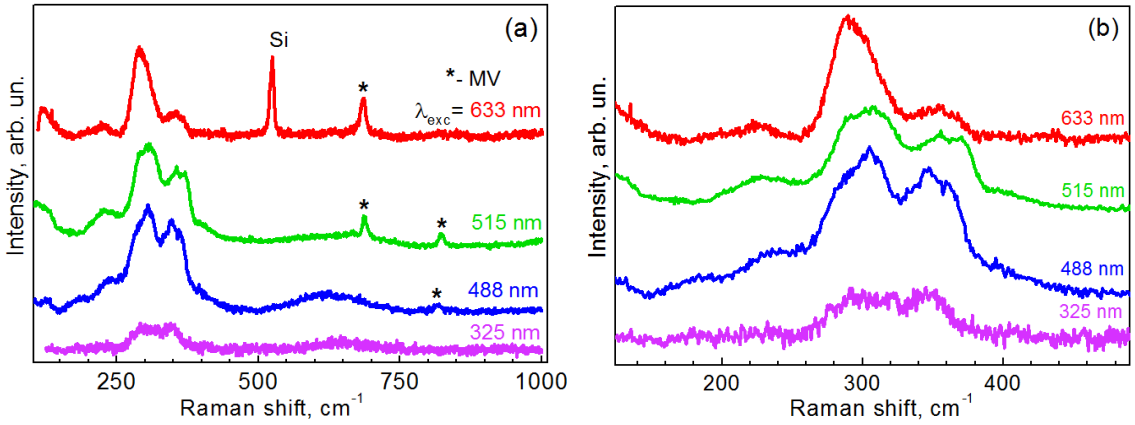

Figure 1. (a) Representative RT Raman spectra of Ag-In-S NCs obtained at different λ_{exc}. The peaks of methyl viologen are marked by asterisks. (b) The first-order phonon range shown in detail.

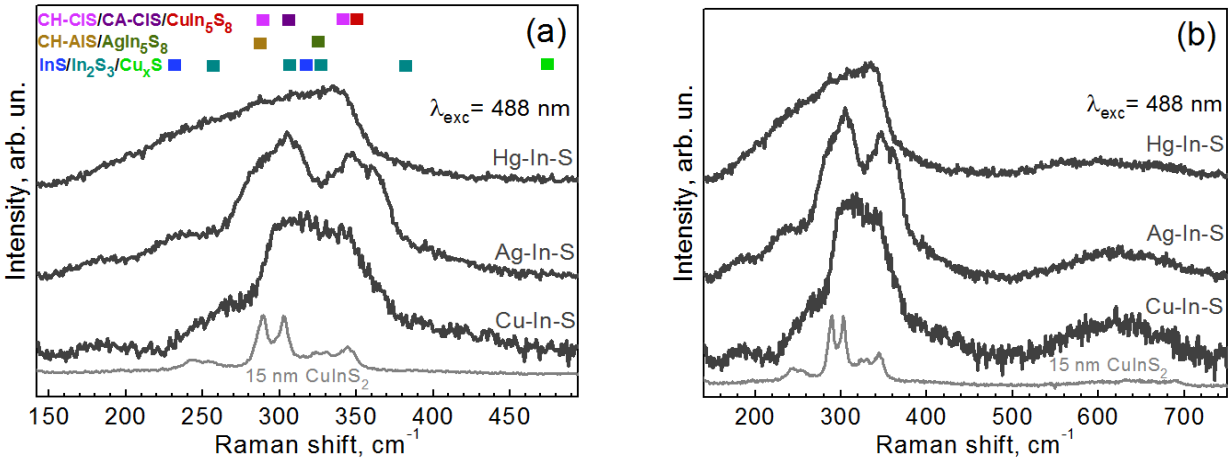

Figure 2. (a) First-order phonon Raman spectra (RT, λ_{exc}=488 nm) of Ag-In-S, Cu-In-S, Hg-In-S 2-4 nm NCs, as well the spectrum of 15 nm $CuInS_2$ NCs [39]. In the upper part, the positions of key modes of main bulk modifications and potentially secondary phases are indicated. (b) The same Raman spectra as in (a) but including the second-order phonon range.

Based on the similarity of the XRD patterns of Hg-In-S, Ag-In-S NCs, and Cu-In-S NCs (Fig. S2, a), the same type of crystalline structure in these three compound NCs can be assumed. From comparing them with calculated XRD patterns of different possible structural modifications (Fig. S2, b) the best matching modification is tetragonal $MInS_2$, in agreement with previous reports for NCs obtained by the same synthesis route [5,6,9,17]. Nevertheless, the reflexes for zinc-blende and wurtzite $MInS_2$, MIn_5S_8, In_2S_3, and InS fall within the width of the XRD features of the M-In-S NCs, and therefore the presence of these secondary phases cannot be excluded based on XRD data only.

Despite presumably similar factors determining position and broadening of Raman and XRD peaks, it is obvious from comparing Fig. 2 and Fig. S2 that the phonon spectra are more specific for the three compound NCs studied. In the following, we will address in more detail several aspects that have the strongest effects on the phonon spectra of the NCs.

Before that, we would like to emphasize several important features of the characterization techniques used. Unlike XRD and XPS, the contribution of different constituent chemical and structural phases to the Raman spectrum of a composite or heterostructure is not necessarily proportional to their atomic or volumetric ratios. They are often determined by the Raman scattering cross-section of a certain bond/vibration and possible resonances of the exciting light with an electronic transition in the given phase [20,28,30]. The effective XRD contribution of large crystallites (roughly above 10 nm) will be much stronger than that of poorly crystalline fragments or very small crystallites. The probing depth of XPS is only several nanometers, so it is a purely surface-sensitive technique for bulk samples, but in the case of 2-4 nm NCs studied here, this technique is suitable to deliver the average NC composition and chemical environment of the constituent atoms. The account of these details is crucially important for the analysis of the corresponding data.

Effect of the non-stoichiometry on the phonon spectra of M-In-S NCs

As was shown in the XPS part, the strongly M-deficient composition of our M-In-S NCs may correspond either to homogeneously M-deficient M-In-S or to a roughly 1:1 mixture of $MInS_2$ and MIn_5S_8. In view of the Cu-deficiency of the Cu-In-S NCs, the absence of Cu_xS features in the Raman spectrum, at about 470 cm^{-1} [40], was quite expected (Fig. 2). We excluded the possibility of a noticeable content of the In_2S_3 phase based on two observations made from comparing the Raman spectra of the three compounds at the same λ_{exc} (Fig. 2). Firstly, a different line shape of the spectra is more expected for three different compounds than for the same one (*i.e.* In_2S_3). Secondly, none of our M-In-S NCs has a feature around the highest frequency expected for In_2S_3, 367 cm^{-1} [41].

Distinguishing the $MInS_2$ and MIn_5S_8 phases is more challenging, due to overlapping ranges of their phonon frequencies and large broadening of the present NC spectra. Nevertheless, one can see from Fig. 2 that the highest bulk mode of $AgIn_5S_8$, 328 cm^{-1}, is 22 cm^{-1} lower than that of $CuIn_5S_8$, 350 cm^{-1} [42], while the Raman spectrum of Ag-In-S NCs extends to higher frequencies than that of Cu-In-S NCs. Based on this fact we can exclude a noticeable content of the MIn_5S_8 phases in our NCs.

Moreover, the presence of two structural modifications in the NCs, *i.e.* $MInS_2$ and MIn_5S_8, would also be detectable in PL spectra, which can be satisfactorily fitted with a single Gauss profile in most cases. If both phases are fluorescent, the resulting spectrum

of M-In-S NCs would be much broader and asymmetric compared to single-phase NCs, because the PL positions of $MInS_2$ and MIn_5S_8 NCs were shown to differ by 200-300 nm or 300-350 meV [43]. Alternatively, if one of the phases were non-fluorescent due to abundance of non-radiative defects/states, this would most likely quench PL of the whole NC, due to exciton delocalization over the whole volume of the NC.

Spectral range of 340-350 cm^{-1}

It should be noted that results and conclusions of previous publications on the relation between the (possible) presence of MIn_5S_8 phase in M-In-S and the lineshape of the Raman spectrum are very contradictory. Some authors concluded on the presence of MIn_5S_8 phase based on observing a strong 340-350 cm^{-1} feature, even for $MInS_2$-stoichiometric [44–46] and very In-poor NCs [44]. Others, on the contrary, observed a very weak [47] or no [48,49] such Raman peak even for strongly Cu-deficient samples (favorable for the formation of an In-rich phase such as $CuIn_5S_8$). A single unreasonably broad (FWHM ~100 cm^{-1}) Raman band at 326 cm^{-1} was reported for 20 nm $CuIn_5S_8$ NCs [50], even though the most pronounced Raman features of $CuIn_5S_8$ are expected at 350 cm^{-1} [42]. The spectra of ≈3 nm $AgInS_2$ NCs reported in Ref. [51] are similar to ours, but their NCs of a similar size identified as $AgIn_5S_8$ possessed a main peak at 290-305 cm^{-1}, *i.e.* at the position of bulk A_1-phonon of $AgInS_2$ [52] and far from the main vibration of bulk $AgIn_5S_8$ at 329 cm^{-1} [42].

A more reasonable assignment of the 340-350 cm^{-1} Raman band, both in Ag-In-S and Cu-In-S, is to E/B(LO) modes of the tetragonal-like structure [39,53–55]. We use the term 'tetragonal-like' because in highly non-stoichiometric NCs the tetragonal lattice gets strongly distorted [7]. The lattice distortion can also be responsible for the activation of phonon modes that are not Raman-active in the ideal tetragonal lattice, as well as for changing of the relative intensities of the Raman-active modes.

An additional strong argument favoring the assignment of the 340-350 cm^{-1} Raman band to the LO mode is a noticeable increase of the relative intensity of this feature at low temperature (Fig. 3). This behavior is similar to that previously found by us for stoichiometric $CuInS_2$ NCs [39].

A-mode around 290-300 cm^{-1}

The most intense and characteristic Raman peak of tetragonal (chalcopyrite) $CuInS_2$ and $AgInS_2$ is the one at about 290 cm^{-1} caused by vibrations of anions with cations at rest [52]. The frequency and FWHM of this Raman peak are sensitive to the crystallinity of the sample and its stoichiometry [56]. The so-called CuAu (CA) structural modification of $CuInS_2$ was identified only by Raman spectroscopy, for which this mode (A_1^*) occurs at 305 cm^{-1} [56], favored for Cu-poor compositions [27,47,55,57–59]. The analogous crystal structure for $AgInS_2$ has not been observed yet, but in the Raman spectrum of our Ag-In-S NCs one can distinctly see that the first of the two major bands consists of at least two components peaked at about 290 and 300 cm^{-1}, respectively (Figs. 2 and Fig.3). The latter can be, therefore, an analog of the A_1^*-mode of $CuInS_2$, observed here for the first time for Ag-In-S compounds. Multi-peak fitting of the most structured NC spectrum allowed up to eleven components to be deconvoluted in the range of first-order phonons, 150-450 cm^{-1} (Fig. 3,c), which is in a good agreement with the number of first order phonons previously reported by us using DFT calculations for stoichiometric $CuInS_2$ [39]. Realistic calculations of highly non-stoichiometric M-In-S NCs, such as those studied in the present work, is a highly challenging problem, not solved yet.

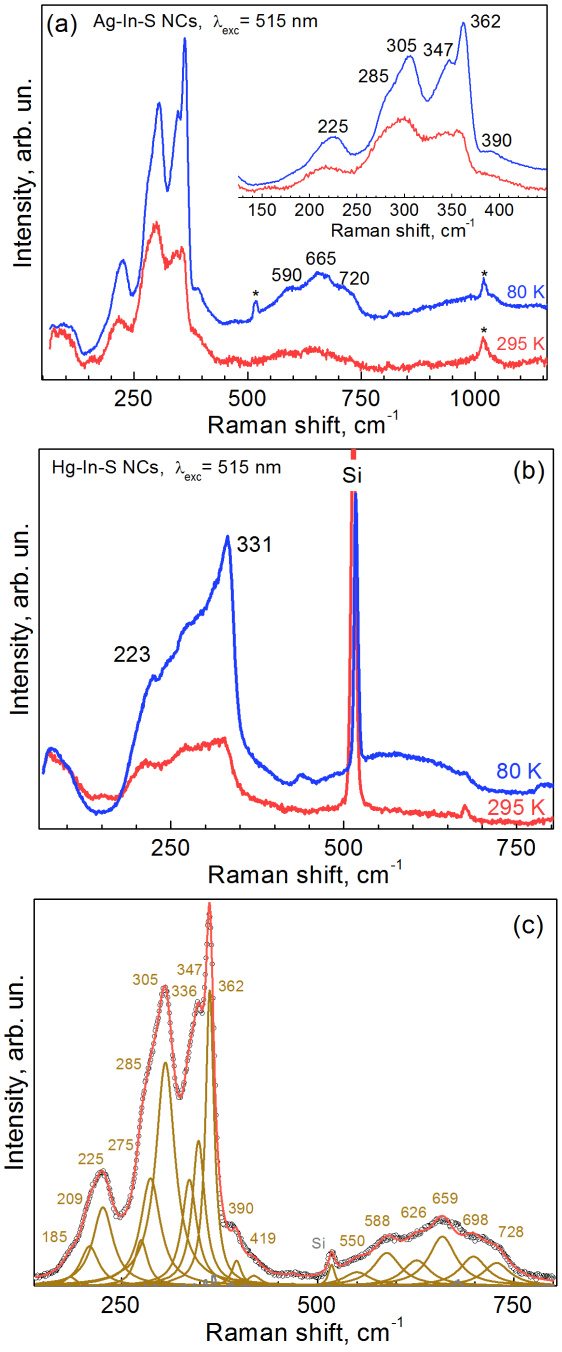

Figure 3. Comparison of the room-temperature (295 K) and low-temperature (80 K) Raman spectra of Ag-In-S (a) and Hg-In-S (b) NCs at λ_{exc}=515 nm. The first-order phonon range of the spectra in (a) is shown in more detail in the inset. Asterisks show features not belonging to the spectra of the NCs. Multiple-peak deconvolution of the Ag-In-S NC spectrum from (a) is shown in (c).

The non-stoichiometric composition can be the reason of the large Raman FWHM (Fig. 2), as compared to bulk crystals and large NCs of nearly ideal stoichiometry (*i.e.* $AgInS_2$, $CuIn_5S_8$, *etc.*). In order to separate the effect of size and non-stoichiometry, we analyzed the evolution of the A_1 Raman mode FWHM with x in $Cu_xIn_{1-x}S$, available in the literature [46,48,49,51,58], but found no unambiguous correlation. Broader Raman peaks are not necessarily observed for NCs or microcrystal films with off- (inter-) stoichiometric composition. Noteworthy is that for I-III-VI NCs synthesized at low temperature and not subjected to post-synthesis thermal annealing/sintering, as in the present work, the detection of phonon Raman spectra was usually not possible, even in the absence of PL, as recognized by some authors [44]. Surprisingly, the latter authors attributed the 345 cm^{-1} peak to the $CuIn_5S_8$ phase even in their very In-poor NC sample. That NC sample possessed also a strong Raman feature of the CA phase, which is more commonly reported for Cu-poor CIS. It is remarkable that the Raman peaks got much sharper in their large ($d = 18$ nm) non-stoichiometric NCs, compared to 2-5 nm stoichiometric ones. This result indicates that the Raman peak width is governed not by the average non-stoichiometry itself but probably by the fact that the NC consists of volumes of stoichiometric compounds like $CuInS_2$ and $CuIn_5S_8$.

Therefore, by excluding many possible "stoichiometric" phases ($AgInS_2$, $CuIn_5S_8$, In_2S_3 *etc.*) are constituents of present M-In-S NCs , we can come to a preliminary conclusion that the Raman peaks broadening is an inherent property of this strongly confined and highly M-deficient system, rather than a result of a multiphase composition. We obtained an additional proof for this conclusion from the analysis of our

low-temperature Raman spectra (Fig. 3). They reveal magnitudes of both the narrowing and upward shift of the phonon features, which are common for "ordinary" (in terms of stoichiometry or larger size) semiconductor NCs such as CdSe [60].

Effect of the monovalent cation on the phonon spectra

Based on the same type of crystal structure in all three compounds, assumed from the above discussion of the Raman spectra and similarity of XRD patterns (Fig. S2), one could expect a qualitative trend of the frequency of a certain phonon mode with the mass of the M (M = Cu, Ag, Au) cation. In this way, the frequency of a certain phonon mode should decrease from Cu (atomic mass $M = 64$) to Ag ($M = 108$) and further to Hg ($M = 201$). However, no such trend can be seen in Fig. 2 or Fig. 3. The highest-frequency feature occurs at nearly the same frequency for Cu-In-S and Hg-In-S, ≈350 cm^{-1}, and at a higher frequency, ≈360 cm^{-1}, for Ag-In-S. Therefore, the relation between the structure of our small NCs and their phonon spectra is obviously more complex. Such complex relation can be interpreted, for example, in the frame of the model proposed by Bhar *et al.* [61], assuming that the frequency of the polar vibration of a particular bond is dependent on the effective charge on the bond, rather than on the elastic constant or the ion mass.

As far as the A_1 mode is concerned, it is a vibration of anions only with no contribution of the motion of cations, and, therefore, not the masses of the cations but the force constants are responsible for the trends of the A_1 mode frequency. As a result, the A_1 mode frequencies are nearly identical for compounds with the same anion and even for compounds with different crystal symmetry [62]. Nevertheless, as the cations with higher masses are normally also bigger and exhibit lower force constants due to the larger distances to the anions, there is a shift of the A_1 mode to lower frequencies with increasing cation mass, serving as a probe of a mean force constant [62]. This was observed, for instance, in a series of compounds $CuBS_2$ for B=Al, Ga, In, where the A_1 vibration shifts from 315 via 312 to 294 cm^{-1}, or in $AGaS_2$ for A=Cu, Ag from 312 to 295 cm^{-1}, or in $AGeP_2$ for A=Zn, Cd from 328 to 321 cm^{-1}.

In the Raman spectra of our Cu-In-S and Ag-In-S NCs, the most pronounced maximum of the scattering intensity is observed at higher frequencies, 300-310 cm^{-1} (Fig. 2,a), with respect to the corresponding A_1-mode position in bulk $AgInS_2$ and $CuInS_2$ (around 290 cm^{-1}). One explanation for this can be a contribution of the CuAu-phase, having its characteristic A_1^* mode at a higher frequency (305 cm^{-1} for $CuInS_2$, see discussion in the previous section). An alternative explanation can be the phonon confinement effect. Even though it usually shifts optical phonon peaks in chalcogenide NCs to lower frequencies [21], an upward shift was also reported for $CuInS_2$ [63] and Cu-Zn-Sn-S NCs [26], and explained by the opposite (positive) dispersion of the highest-frequency optical phonon branches in these materials. Note that an upward shift of the phonon modes occurring due to structural reconstruction in ultrasmall NCs was reported for CdS and CdSe [64].

Therefore, the observed lineshape of the phonon Raman spectra of the three M-In-S NC systems is generally consistent with their rather small size and significant non-stoichiometry (with respect to the known bulk modifications). In view of the very close FWHM of the XRD reflexes of all three NC compounds (Fig. S2,a), only a tentatively stronger structural disorder in Hg-In-S, compared to Ag-In-S and Cu-In-S (inferred from the slightly broader XRD reflexes), cannot be sufficient to explain much more broadened Raman lineshape of the former.

Apparently, we have to assume other effects playing a significant role in determining the (different) Raman phonon lineshapes in these small NC compounds – presumably, different effective charges, phonon anharmonicity, and electron-phonon coupling. Our temperature-dependent Raman spectra did not reveal any drastic difference in narrowing of the Ag-In-S and Hg-In-S spectra with temperature decrease. The conclusion about the EPC resonance effects are discussed below.

Resonance effects in the Raman spectra and EPC

As already mentioned above, our preferred assignment of the band around 340-350 cm^{-1}, which is most pronounced for Ag-In-S NCs (Fig. 2), is a E^1/B_2^1(LO) of tetragonal-like M-In-S [57]. According to polar nature of LO modes, their resonant enhancement is expected at near-bandgap excitation, which often facilitates their assignment [39,55,65]. It should be noted, however, that in the case of the featureless optical absorption spectra of I-III-VI_2 NCs, the existence of pronounced resonant conditions is questionable. Nevertheless, it was shown earlier that excitation of large (above 10 nm) stoichiometric $CuInS_2$ NCs, showing a similarly featureless absorption band edge, with 750-785 nm laser lines results in a much higher relative intensity of this B_2(LO)/E(LO) Raman band, compared to A_1-mode(s), as well as the observation of LO overtones and combination tones of different LO modes [39,55,66]. It should be noted, however, that the 2LO/LO ratio for $CuInS_2$ NCs was 10-20 times lower than for bulk $CuInS_2$ at the same λ_{exc} [66]. This may simply reflect a shift of electronic transitions in the NCs away from the resonance with λ_{exc}. Alternatively, this can be a part of a general property/trend consisting in a weaker EPC of LO modes with the excited electronic state in strongly confined NCs due to a reduced polarity of the exciton [21,67–70]. The strong EPC strength in the emitting exciton state, which manifests itself in the PL spectra and inferred from the STE model [11], may be due to different symmetry and spatial localization of the electron wave function compared to the excited state participating in the Raman process.

The most pronounced difference in the resonant behavior of the present NCs compared to bulk $CuInS_2$ is related to opposite trends in the relative intensity of the 350 cm^{-1} mode: in bulk Cu-In-S it gets strongly enhanced towards longer λ_{exc} [39], while we observe a distinct opposite trend (Fig. 1). The relative intensity of I_{LO}/I_{A1} at λ_{exc} = 785 nm does not differ much from that at λ_{exc} = 633 nm. We may assume that in the stoichiometric bulk crystals and large NCs, the latter excitation condition is more resonant with excitonic states. In the case of our highly non-stoichiometric and strongly confined NCs, the absorption edge is formed by disorder-related states (the Urbach tail) [71], and excitation in these states may result in a lower overall Raman intensity and a relatively lower intensity of extended optical (LO) modes. The 785 nm excitation is, in turn, well below the resonance with interband transitions, explaining the low I_{LO}/I_{A1} ratio.

Investigating and understanding the resonant behavior of the Raman spectra helps in clarifying the nature of modes. In particular, it is known that the A_1 mode does not produce second-order Raman peaks even at resonant excitation, while overtones and combination tones of LO modes are readily observed [39]. Under appropriate resonant conditions, their intensity can even exceed that of the first-order peaks [55]. These conclusions are well proved by resonant Raman studies on $CuGaS_2$ [66,72], which was more intensively investigated compared to Cu-In-S and Ag-In-S. For $CuInS_2$ multiphonon spectra were previously reported only in [39,55], but analyzed only in our

previous work on stoichiometric 15 nm wurtzite $CuInS_2$ NCs [39]. Resonant enhancement of LO modes and related higher-order Raman scattering is a general property of polar modes in various semiconductor compounds, explained by the Fröhlich electron-phonon coupling mechanism [73–75]. In the spectra of the present M-In-S NCs a clear second-order feature is observed at ≈ 650-700 cm^{-1} (Figs. 2b, 3, 4b), and its intensity correlates with the intensity of the feature around 350 cm^{-1}. In the low-temperature spectra, we succeeded to resolve at least three components in the second-order phonon range (Fig. 3), with the following tentative assignment: 225 cm^{-1}+362 cm^{-1}→590 cm^{-1}, 305 cm^{-1}+362 cm^{-1}→665 cm^{-1}, 2×362 cm^{-1}→720 cm^{-1}. This behavior is an additional solid argument in favor of the B_2(LO)/E(LO) origin of the 340-350 cm^{-1} band, rather than its assignment to the non-polar A_1-mode of MIn_5S_8. Remarkable is the fact that the relative intensity of the second-order scattering, which is proportional to the strength of the electron-optical phonon coupling via the Fröhlich mechanism [70,73–75], is stronger in our NCs compared to stoichiometric and larger $CuInS_2$ NCs (Fig. 2b). Even in the Hg-In-S spectrum, with hardly discernible vibrational structure (Fig. 2b), the second-order band is observable (≈590 cm^{-1}). This can be a further argument supporting our recent hypothesis about the self-trapped exciton mechanism of the strong PL emission of the given type of NCs, which particularly demands the assumption of strong EPC [11].

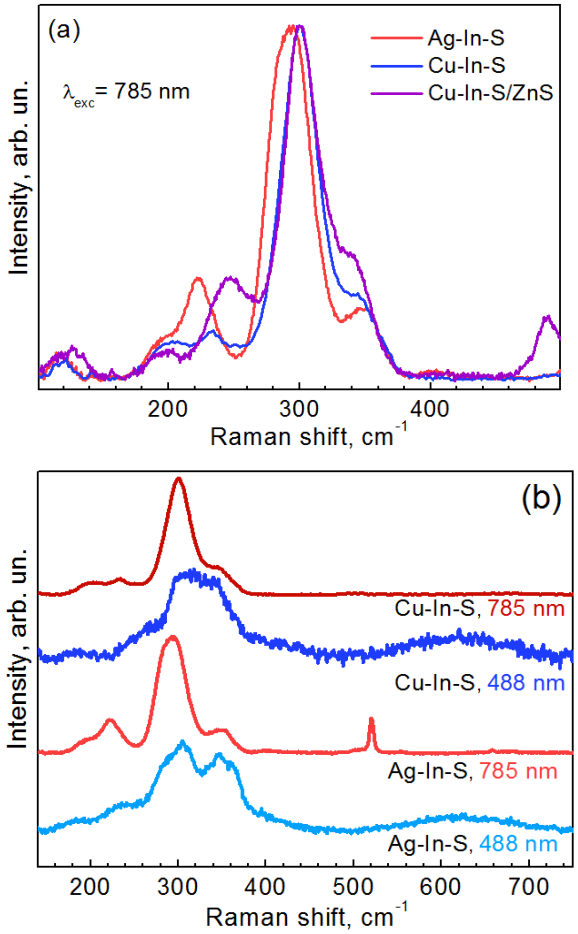

Figure 4. (a) First-order phonon range of the Raman spectra of Ag-In-S, Cu-In-S, and Cu-In-S/ZnS NCs at λ_{exc}=785 nm. (b) Comparison of the Raman spectra of Ag-In-S and Cu-In-S NCs at λ_{exc}=785 nm and λ_{exc}=488 nm.

Size and surface effects

Contrary to II-VI, III-VI, and IV-VI NCs, where small but distinct and regular optical phonon shift and broadening were observed with decreasing NC size below ≈5 nm [67–69], the observation of phonon confinement in I-III-VI NCs is strongly precluded by their non-stoichiometry, lattice distortion, and weak dispersion of optical phonons. For this reason, as already mentioned, the reports on Raman peak positions and widths of phonons localized in different NC sizes are

contradictory. Obviously, any assessment of the magnitude of the phonon confinement effect is only allowed/reasonable when comparing NCs and bulk material with the same composition. As long as the corresponding bulk references are not available, any assessment of phonon confinement in NC samples is not reliable (cannot be verified).

Surface optical phonon modes, expected between the zone-center TO and LO phonon frequency and regularly observed for binary NCs even larger than 5 nm [21,76], cannot be distinguished in I-III-VI NCs due to the large number of modes, their larger FWHM, as well as smaller TO-LO splitting.

IR spectra of M-In-S NCs

A further insight into the understanding of the phonon spectra and possibly their relation to the NC structure can be obtained from IR spectra (Fig. 5). Generally, IR spectra are considered as complementary to Raman, based on different selection rules. Usually polar TO phonons are active in IR, while fully symmetric vibrations give strongest peaks in Raman scattering (the A_1 mode is a good example for the M-In-S compounds). Due to the resonant nature of Raman spectra in this work and the non-stoichiometrical phases, they may contain modes that are expected in the IR spectra only. The experimental IR spectra of the Ag-In-S and Cu-In-S NCs reveal main features (227, 300, and 345 cm^{-1}) in the same range as the Raman spectra, but, compared to Raman spectra, they show more similarity between the two compounds and with spectra of bulk $MInS_2$ and MIn_5S_8 from the literature [42,62,77–82].

We observe a good qualitative correlation (*i.e.* the number and positions of main features) between the spectra of the same sample measured in classical reflection and attenuated total reflection (ATR) geometries. Therefore, the representative spectra of Ag-In-S and Cu-In-S NCs in Fig. 5 are shown for different geometries, enabling comparison with corresponding spectra from the literature [42,52].

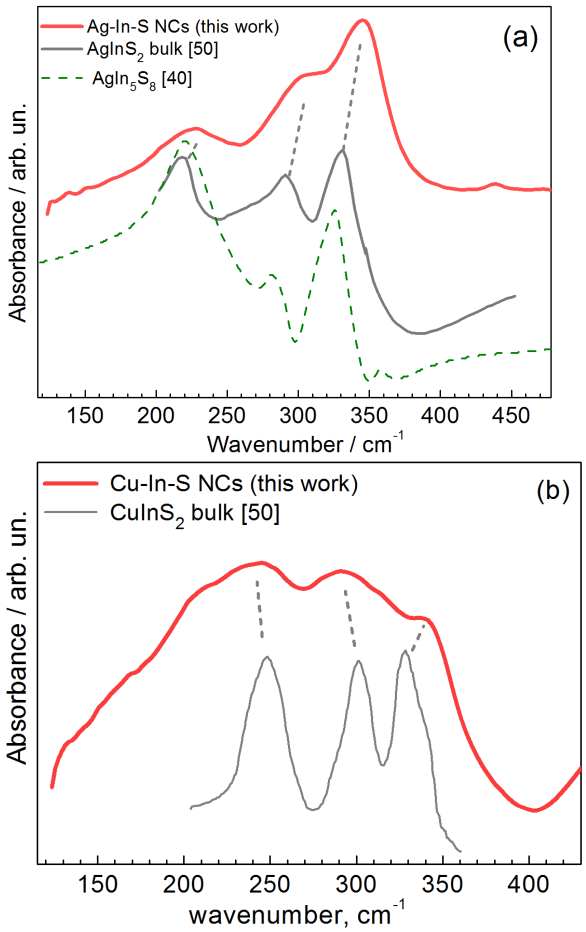

Figure 5. Infrared phonon spectra of Ag-In-S (a) and Cu-In-S (b); NCs in comparison with the spectra of bulk $AgInS_2$ [52] and $CuInS_2$ [52], and $AgIn_5S_8$ [42].

We observe a good correlation between the IR and Raman spectra of our NCs, confirming the assignment of the modes made in the previous sections. In particular, the highest-frequency and strongest IR mode of Ag-In-S NCs, at 352 cm^{-1}, and of Hg-In-S NCs, at 335 cm^{-1}, correlate well with the corresponding position of Raman peaks at 340-350 cm^{-1} and their assignment to polar (LO) modes of tetragonal-like M-In-S rather than A-mode of

MIn_5S_8. The main IR modes of bulk $AgIn_5S_8$ occur at 83, 207, 278, and 313 cm^{-1} [82].

Less characteristic is the IR mode at 225 cm^{-1} (also in Raman), which is related to the vibration of In-S bonds common for all the three compounds. Only at λ_{exc} = 785 nm we observe a shift of this feature to 220 cm^{-1} for Ag-In-S and to 230 cm^{-1} for Cu-In-S (Fig. 4a).

Probably most interesting is the presence of the band at ≈300 cm^{-1} in the IR spectra for all M-In-S NC compounds (Fig. 5) because this is the range of the presumably most strong Raman-active A_1-mode. However, in view of a relatively strong and broad second-order Raman band (for all M-In-S NCs compounds) (Fig. 3), we may assume contribution of LO modes to the Raman spectrum in the range of ≈300 cm^{-1} as well. This could be an additional factor explaining the broadening of the first-order Raman spectra.

The most intense bands in the IR-spectra of chalcopyrites are normally characterized by B_2^1-, B_2^2-, E_1- and E_3-symmetry, as can be seen from comparison of our DFT-modelled with experimental IR spectra (Fig. 6). A good overall agreement between the calculated positions of the IR-active modes and the maxima in the experimental IR spectra can be noticed (Fig. 6).

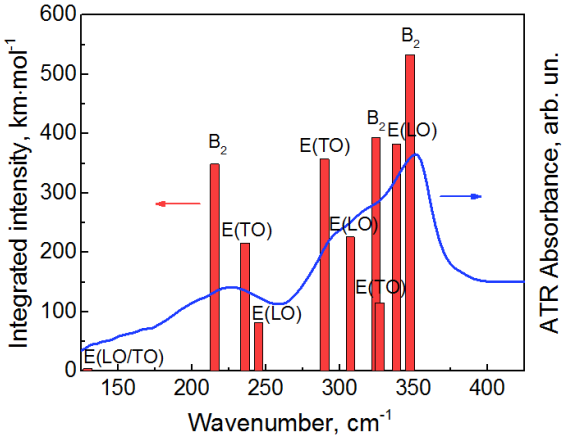

Figure 6. DFT calculations of IR active modes (vertical bars) for tetragonal $AgInS_2$ lattice superimposed on the experimental IR spectrum of AIS QDs (solid line).

Effect of Zn shell/alloying

Forming a higher-bandgap shell is a well-known approach to increase the PL of colloidal NCs and improve its stability against oxidation [83]. The same effect was observed for M-In-S NCs, with PL QY increasing from 14 % for AIS NCs up to 60 % for AIS/ZnS NCs [11]. From previous reports on different core/shell systems it is known that the spectral changes induced by adding shell are not always the same and strongly dependent on the mechanism of Zn incorporation [84]. A red shift in PL and UV-vis absorption spectra upon adding a shell indicates its regular formation as additional monolayers around the (core) NC [83]. In case of blue shifts in the optical spectra, one obtains partial or complete alloying of the shell material with the core [1]. The latter scenario is markedly observed for our MIS/ZnS NCs (Fig. S1). Therefore, the increase of the PL intensity in this case is not only due to forming the potential barrier around the core, but probably also due to eliminating non-radiative defects inside the core. For M-In-S NC PL, which presumably combines properties of excitonic and trap-related emission (in the STE model), the relation between the lattice structure and the PL spectra still lacks a deep understanding. This is an additional motivation to explore the modification of phonon spectra of the three M-In-S NC systems upon incorporation of Zn from the ZnS shell.

A comparison of XPS data of core vs core/shell NCs of all three systems provides additional information about the structure and distribution of elements within the NCs, as well as sheds light on the mechanism of NC stabilization by ligands. The latter is not straightforward for such relatively complex systems and may differ substantially for the three M-In-S NC compounds. In our case, XPS data show that at close (M+In)/Zn ratios in all three core/shell systems, Ag:In and

Hg:In ratios are preserved in core/shell NCs, while Cu:In is notably reduced. This difference may be explained by weaker in-diffusion of Zn into CIS core compared with AIS and HIS ones. The resulting Zn-enriched surface in CIS/ZnS NCs, compared to a more smooth Zn gradient for AIS/ZnS and HIS/ZnS, can be seen in XPS as Zn-richer or Cu-poorer NCs. This presumably less intense alloying can be responsible for the smaller PL blue shift, related with adding ZnS, in case of CIS/ZnS (0.08 eV) compared with AIS/ZnS (0.20 eV) and HIS (0.14 eV) (Fig. S1). Nevertheless, this weaker alloying does not lead to the formation of noticeable pure ZnS shell on CIS NCs, as can be seen from the similarity of the Zn-S vibration peak in the UV Raman spectra of all three NC compounds (Fig. 7b). The IR spectra of all the three systems also look very similar as well, as discussed below (Fig. 7c).

The present results are in accordance with the observation from our previous work on Cu-doped AIS-TGA NCs [5]. There, we observed the expected blue shift of AIS absorption and PL bands after the deposition of a ZnS shell. However, if we doped AIS with Cu, we did not observe any shift after the deposition of ZnS. We explained it by a simplified model that Cu ions assumedly fill vacancies precluding Zn^{2+} ions from incorporating in the core, but there could also be an alloyed CAIS layer on the QD surface and this surface alloy cannot be easily penetrated by Zn^{2+}.

No major difference in the Raman spectra of Hg-In-S and Hg-In-S/ZnS NCs excited with visible light (488, 515, 633 nm; the case of λ_{exc} = 488 nm is shown in Fig. 7a) can be explained by the resonance with core-related electronic transitions, resulting in the dominance of core-related phonons in the spectra of core/shell NCs as well. Same situation we observed recently for Zn-Cu-In-S and Zn-Cu-In-S/ZnS NCs [18]. The only apparent difference between the present Raman spectra of Hg-In-S and Hg-In-S/ZnS NCs in Fig. 7a is the higher relative intensity in the range of 300 to 350 cm-1 for Hg-In-S sample may be related with stronger intensity of the LO modes due to a more favorable resonance conditions of λ_{exc}=488 nm for this sample, as compared to the Hg-In-S/ZnS, with a blue shifted absorption onset (Fig.S1).

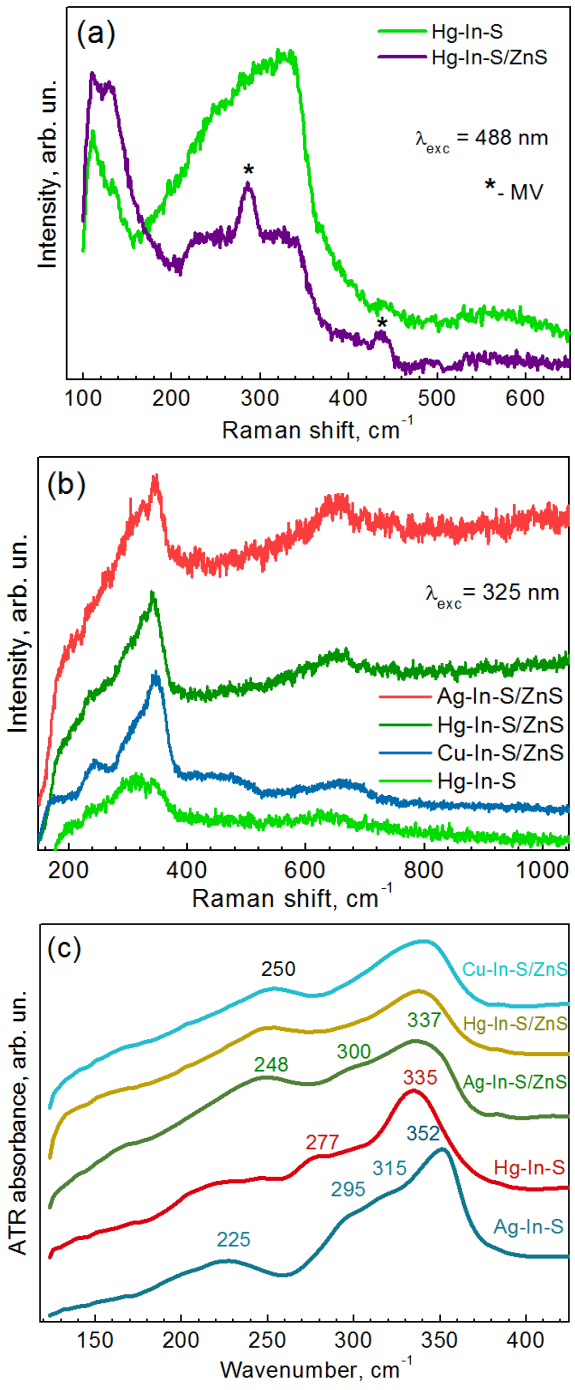

Figure 7. (a) RT phonon Raman spectra of Hg-In-S and Hg-In-S/ZnS NCs at $\lambda_{exc} = 488$ nm; (b) Raman spectra of Hg-In-S, Hg-In-S/ZnS, Cu-In-S/ZnS, and Ag-In-S/ZnS NCs at $\lambda_{exc} = 325$ nm; (c) ATR-IR phonon spectra of Ag-In-S, Hg-In-S, Ag-In-S/ZnS, Hg-In-S/ZnS, and Cu-In-S/ZnS core/shell NCs.

This also indicates that addition of ZnS results mainly in NC alloying but not in the formation of a ZnS shell. Such a resonant selectivity of the Raman scattering was systematically studied for II-VI core/shell NCs [21] as well as for more complex compound semiconductor NCs, such as $CuInS_2$ and $CuInS_2$/ZnS, Zn-Cu-In-S and Zn-Cu-In-S/ZnS [18]. For the latter systems, it was shown that the detection of the shell-related phonons in the Raman spectra was possible only using UV excitation, 325 nm [18], which is resonant with the ZnS bandgap. Raman spectra taken at the UV excitation in Fig. 5b do not reveal a ZnS LO phonon peak (expected at 345-350 cm^{-1} in the NCs, depending on their size [18,85], but instead show a broad feature, asymmetrically broadened towards lower frequencies, indicative of Zn-S bond distribution in an alloy [86].

Due to a significant increase of the PL intensity in core/shell NCs, it was possible to acquire Raman spectra at visible excitation only for Hg-In-S/ZnS NCs (Fig. 7). For the other two core/shell systems, we analyzed only the Raman spectra at 325 nm (Fig. 5b), 785 nm (Fig. 4) excitations, as well as IR phonon spectra (Fig. 5).

The IR spectra of Hg-In-S/ZnS NCs reveal distinct peaks at 250 and 338 cm^{-1} (Fig. 7c). The latter could be a 335 cm^{-1} feature of bare Hg-In-S NCs, slightly shifted to higher frequencies and broadened by shell-induced strain and Zn-alloying. Earlier, we observed by IR and Raman spectroscopies the development of strain in CdSe cores, induced by the lattice mismatch with CdS or ZnS shells [20–22]. On the other hand, the feature at 338 cm^{-1} matches well the range of SO phonon reported for ZnS NCs [85]. Moreover, in the spectra of all our core/shell NCs, another core mode, at 220-240 cm^{-1}, is apparently transformed into a mode at 250 cm^{-1} (Fig. 7c). Even though the latter peak is below the TO mode (the lowest optical frequency) of ZnS (bulk ≈275 cm^{-1} [87]), it can be a hybrid interface mode of these M-In-S/ZnS NCs, modified by more intense Zn diffusion into the core. A strong additional proof favoring the assignment of both 250 and 338 cm^{-1} IR peaks of the core/shell NCs to (alloyed) shell was the observation of very similar spectra for all three similarly synthesized core/shell NCs (Fig. 7c), despite noticeable differences between the spectra for the three bare NC systems (Ag-In-S, Cu-In-S, and Hg-In-S) (Fig. 3 and Fig. 7c).

Conclusions

A detailed analysis of phonon spectra of strongly luminescent colloidal M-In-S (M=Cu, Ag, Hg) and M-In-S/ZnS NCs of small size ($d \approx 3$ nm) was performed. We established the relation between the optically active lattice vibrations and lattice structure and found the phonon spectra to be more sensitive to the NC composition and crystalline structure, compared to XRD patterns.

Based on the comparison of our experimental Raman spectra, measured at different λ_{exc} and temperatures, with those of corresponding stoichiometric phases, *e.g.* $CuInS_2$ or $AgIn_5S_8$, and potential binary sulfides, *e.g.* In_2S_3, we conclude that the Raman spectra observed are characteristic of the specific structure of these highly non-stoichiometric small NCs. Particularly, we resolved one of the major discrepancies in the literature, the interpretation of the Raman phonon mode(s) in the range of 340-350 cm^{-1}, and show that the latter are not due to MIn_5S_8

as a secondary phase but the LO modes of the tetragonal structure, corroborating our XRD results.

Both the low-temperature and second-order Raman spectra of Ag-In-S NCs are reported here for the first time. Combination of these data was crucial for suggesting the combinations of the first-order phonons that may form the second-order scattering spectrum. It is remarkable that the second-order scattering is only possible with participation of LO phonons – either as purely LO overtones or combination of LO and A_1-modes.

Furthermore, we suggest for the first time a phonon feature observed in the Raman spectrum of Ag-In-S NCs is related to the structural analog of the CuAu phase reported earlier only for Cu-In-S.

IR spectra of the M-In-S NCs are less characteristic, revealing more similarity among the three NC compounds and with bulk counterparts, and are corroborated by our DFT calculations. Similar changes in both the Raman and IR spectra of all three compound NCs upon adding ZnS shell, accompanied by its partial alloying with the M-In-S core, additionally confirm the structural similarity of the three NC compounds and their structural difference from the bulk counterparts. The combination of XPS and resonant Raman spectroscopy with UV (325 nm) excitation proved to be efficient in distinguishing strongly alloyed and clearly heterogeneous structures of core/shell NCs in strongly confined and non-stoichiometric nanosystems like the M-In-S/ZnS NCs studied.

Supporting Information. UV-vis, PL, XRD, and XPS data on the samples investigated are available free of charge.

Corresponding Author

* Volodymyr Dzhagan, V. Lashkaryov Institute of Semiconductors Physics, National Academy of Sciences of Ukraine, Nauky av., 03028 Kyiv, Ukraine; Taras Shevchenko National University of Kyiv, 64 Volodymyrs'ka St., 01601 Kyiv, Ukraine; dzhagan@isp.kiev.ua

Author Contributions

The manuscript was written through contributions of all authors. All authors have given approval to the final version of the manuscript.

Acknowledgment

The work was partially supported by Volkswagen Foundation (project “New functionalities of semiconductor nanocrystals by controllable coupling to molecules”), and NAS of Ukraine (project 05-02-2020 "Investigation of the features of cationic substitution in nanocrystals of quadruple metal chalcogenides - materials of the new generation of thin-film photovoltaics") as well as DFG ZA 146/45-1 “Environment-friendly 0D/2D nanocomposites for broadband UV-vis-NIR-sensitive photodetectors”.

Abbreviations

XPS, X-ray photoemission spectroscopy; LO phonon, longitudinal optical phonon; MAA, mercaptoacetic acid; STE, self-trapped exciton; EPC, electron-phonon coupling.

References

[1] Aldakov D, Lefrançois A and Reiss P 2013 Ternary and quaternary metal chalcogenide nanocrystals: synthesis, properties and applications *J. Mater. Chem. C* **1** 3756–3776

[2] Knowles K E, Hartstein K H, Kilburn T B, Marchioro A, Nelson H D, Whitham P J and Gamelin D R 2016 Luminescent Colloidal Semiconductor Nanocrystals Containing Copper: Synthesis, Photophysics, and Applications *Chem. Rev.* acs.chemrev.6b00048

[3] Sandroni M, Wegner K D, Aldakov D and Reiss P 2017 Prospects of Chalcopyrite-Type Nanocrystals for Energy Applications *ACS Energy Lett.* **2** 1076–88

[4] Stroyuk O, Raevskaya A and Gaponik N 2018 Solar light harvesting with multinary metal chalcogenide nanocrystals *Chem. Soc. Rev.* **47** 5354–422

[5] Raevskaya A, Rozovik O, Novikova A, Selyshchev O, Stroyuk O, Dzhagan V, Goryacheva I, Gaponik N, Zahn D R T and Eychmüller A 2018 Luminescence and photoelectrochemical properties of size-selected aqueous copper-doped Ag-In-S quantum dots *RSC Adv.* **8** 7550–7557

[6] Raevskaya A, Lesnyak V, Haubold D, Dzhagan V, Stroyuk O, Gaponik N, Zahn D R T and Eychmüller A 2017 A Fine Size Selection of Brightly Luminescent Water-Soluble Ag-In-S and Ag-In-S/ZnS Quantum Dots *J. Phys. Chem. C* **121** 9032–42

[7] Berends A C, Mangnus M J J, Xia C and Rabouw F T 2019 Optoelectronic Properties of Ternary I–III–VI2 Semiconductor Nanocrystals: Bright Prospects with Elusive Origins *J. Phys. Chem. Lett.* **10** 1600–16

[8] Anand A, Zaffalon M L, Gariano G, Camellini A, Gandini M, Brescia R, Capitani C, Bruni F, Pinchetti V, Zavelani-rossi M, Meinardi F, Crooker S A and Brovelli S 2019 Evidence for the Band-Edge Exciton of CuInS 2 Nanocrystals Enables Record Efficient Large-Area Luminescent Solar Concentrators *Adv. Funct. Mater.* 1906629

[9] Stroyuk O, Raevskaya A, Spranger F, Selyshchev O, Dzhagan V, Solonenko D, Gaponik N, Zahn D R T and Eychmüller A 2019 Mercury-indium-sulfide nanocrystals : A new member of the family of ternary in based chalcogenides Mercury-indium-sulfide nanocrystals : A new member of the family of ternary in based chalcogenides *J. Chem. Phys.* **151** 144701

[10] Stroyuk O, Dzhagan V, Raevskaya A, Spranger F, Gaponik N and Zahn D R T 2019 Insights into different photoluminescence mechanisms of binary and ternary aqueous nanocrystals from the temperature dependence : A case study of CdSe and Ag-In-S *J. Lumin.* **215** 116630

[11] Stroyuk O, Raevskaya A, Spranger F, Selyshchev O, Dzhagan V, Schulze S, Zahn D R T and Eychmüller A 2018 Origin and Dynamics of Highly Efficient Broadband Photoluminescence of Aqueous Glutathione-Capped Size-Selected Ag-In-S Quantum Dots *J. Phys. Chem. C* **122** 13648–58

[12] Baimuratov A S, Martynenko I V, Baranov A V, Fedorov A V, Rukhlenko I D and Kruchinin S Y 2019 Giant Stokes Shifts in AgInS2 Nanocrystals with Trapped Charge Carriers *J. Phys. Chem. C* **123** 16430–8

[13] Martynenko I V, Baimuratov A S, Weigert F, Soares J X, Dhamo L, Nickl P, Doerfel I, Pauli J, Rukhlenko I D, Baranov A V and Resch-genger U 2019 Photoluminescence of Ag – In – S / ZnS quantum dots : Excitation energy dependence and low-energy electronic structure *Nano Res.* **12** 1595–1603

[14] Hamanaka Y, Ozawa K and Kuzuya T 2014 Enhancement of Donor − Acceptor Pair Emissions in Colloidal AgInS 2 Quantum Dots with High Concentrations of Defects *J. Phys. Chem. C* **118** 14562−14568

[15] Stroyuk O, Weigert F, Raevskaya A, Spranger F, Wu C, Gaponik N and Zahn D R T 2019 Inherently Broadband Photoluminescence in Ag-In-S/ZnS Quantum Dots Observed in Ensemble and Single-Particle Studies *J. Phys. Chem. C* **123** 2632–41

[16] Wakita K, Ohta Y and Ogushi N 2007 Time-resolved study of resonant secondary

emission on CuInS2 crystals *Thin Solid Films* **515** 6269–71

[17] Raevskaya A, Rosovik O, Kozytskiy A, Stroyuk O, Dzhagan V and Zahn D R T 2016 Non-stoichiometric Cu–In–S@ZnS nanoparticles produced in aqueous solutions as light harvesters for liquid-junction photoelectrochemical solar cells *RSC Adv.* **6** 100145–57

[18] Dzhagan V, Kempken B, Valakh M, Parisi J, Kolny-Olesiak J and Zahn D R T 2017 Probing the structure of $CuInS_2$-ZnS core-shell and similar nanocrystals by Raman spectroscopy *Appl. Surf. Sci.* **395** 24–8

[19] Lox J F L, Dang Z, Dzhagan V M, Spittel D, Martín-García B, Moreels I, Zahn D R T and Lesnyak V 2018 Near-Infrared Cu-In-Se-Based Colloidal Nanocrystals via Cation Exchange *Chem. Mater.* **30** 2607–17

[20] Dzhagan V, Milekhin A G, Valakh M Y, Pedetti S, Tessier M, Dubertret B and Zahn D R T 2016 Morphology-induced phonon spectra of CdSe/CdS nanoplatelets: core/shell vs. core-crown *Nanoscale* **8** 17204–12

[21] Dzhagan V M, Azhniuk Y M, Milekhin A G and Zahn D R T 2018 Vibrational spectroscopy of compound semiconductor nanocrystals *J. Phys. D Appl. Phys.* **51** 503001

[22] Lange H, Machón M, Artemyev M, Woggon U and Thomsen C 2007 Effect of ZnS shell on the Raman spectra from CdSe nanorods *Phys. Status Solidi - Rapid Res. Lett.* **1** 274–6

[23] Silva A C A, Neto E S F, da Silva S W, Morais P C and Dantas N O 2013 Modified Phonon Confinement Model and Its Application to CdSe/CdS Core–Shell Magic-Sized Quantum Dots Synthesized in Aqueous Solution by a New Route *J. Phys. Chem. C* **117** 1904–14

[24] Silva A C A, Silva S W da, Morais P C and Dantas N O 2014 Shell Thickness Modulation in Ultrasmall CdSe/CdSxSe1-x/CdS Core/Shell QuantumDots via 1-Thioglycerol *ACS Nano* **8** 1913–22

[25] Havryliuk Y, Selyshchev O, Valakh M Y, Raevskaya A, Stroyuk O, Schmidt C, Dzhagan V and Zahn D R T 2019 Raman study of flash lamp annealed aqueous Cu2ZnSnS4 nanocrystals *Beilstein J. Nanotechnol.* **10** 222–7

[26] Havryliuk Y, Valakh M Y, Dzhagan V, Greshchuk O, Yukhymchuk V, Raevskaya A, Stroyuk O, Selyshchev O, Gaponik N and Zahn D R T 2018 Raman characterization of Cu_2ZnSnS_4 nanocrystals: phonon confinement effect and formation of CuxS phases *RSC Adv.* **8** 30736

[27] Álvarez-Garca J, Pérez-Rodrguez A, Romano-Rodrguez A, Morante J R, Calvo-Barrio L, Scheer R and Klenk R 2014 Microstructure and secondary phases in coevaporated CuInS 2 films : Dependence on growth temperature and chemical composition *J. Vac. Sci. Technol. A* **19** 232

[28] Freitas Neto E S, da Silva S W, Morais P C and Dantas N O 2013 Multiphonon Raman Scattering in Coupled Cd 1– x Mn x S Nanoparticles: Magnetic Doping and Thermal Annealing *J. Phys. Chem. C* **117** 657–62

[29] Neto E S F, Silva A C A, Silva S W, Morais P C, Gómez J A, Baffa O and Dantas N O 2013 Raman spectroscopy of very small Cd 1 - x Co x S quantum dots grown by a novel protocol : direct observation of acoustic-optical phonon coupling *J. Raman Spectr.* **44** 1022–32

[30] Fairbrother A, Izquierdo-Roca V, Fontané X, Ibáñez M, Cabot A, Saucedo E and Pérez-Rodríguez A 2014 ZnS grain size effects on near-resonant Raman scattering: optical non-destructive grain size estimation *CrystEngComm* **16** 4120

[31] Dimitrievska M, Fairbrother A, Saucedo E, Pérez-Rodríguez A and Izquierdo-Roca V 2015 Influence of compositionally induced defects on the vibrational properties of device grade Cu2ZnSnSe4 absorbers for kesterite based solar cells *Appl. Phys. Lett.* **106** 073903

[32] Dimitrievska M, Gurieva G, Xie H, Carrete A, Cabot A, Saucedo E, Pérez-

Rodríguez A, Schorr S and Izquierdo-Roca V 2015 Raman scattering quantitative analysis of the anion chemical composition in kesterite Cu2ZnSn(SxSe1-x)4 solid solutions *J. Alloys Compd.* **628** 464–70

[33] Stroyuk O L, Rayevska O Y, Kozytskiy A V and Kuchmiy S Y 2010 Electron energy factors in photocatalytic methylviologen reduction in the presence of semiconductor nanocrystals *J. Photochem. Photobiol. A Chem.* **210** 209–14

[34] Giannozzi P, Baroni S, Bonini N, Calandra M, Car R, Cavazzoni C, Ceresoli D, Chiarotti G L, Cococcioni M, Dabo I, Corso A D, Gironcoli S De, Gerstmann U, Gougoussis C, Kokalj A, Lazzeri M, Martin-samos L, Marzari N, Mauri F, Mazzarello R, Paolini S, Pasquarello A, Paulatto L and Sbraccia C 2009 QUANTUM ESPRESSO: a modular and open-source software project for quantum simulations of materials *J. Phys. Condens. Matter.* **21** 395502

[35] Giannozzi P, Andreussi O, Brumme T, Bunau O, Nardelli M B, Calandra M, Car R, Cavazzoni C, Ceresoli D, Cococcioni M, Colonna N, Carnimeo I, Corso A D, Gironcoli S de, Delugas P, Jr R A D, Ferretti A, Floris A, Fr G, Wu X and Baroni S 2017 Advanced capabilities for materials modelling with Q uantum ESPRESSO *J. Phys. Condens. Matter.* **29** 465901

[36] Merkys A, Chateigner D, Das A, Serebryanaya N R, Moeck P, Lutterotti L, Quiro M, Downs R T and Bail A Le 2012 Crystallography Open Database (COD): an open-access collection of crystal structures and platform for world-wide collaboration *Nucleic Acids Res.* **40** D420–7

[37] Richter H and Wang Z P 1981 The one phonon Raman spectrum in microcrystalline silicon *Solid State Commun.* **21** 625–9

[38] Forstert M, Girling R B and Hester R E 1982 Infrared, Raman and Resonance Raman Investigations of Methylviologen and its Radical Cation *J. Raman Spectrosc.* **12** 36–48

[39] Dzhagan V M, Litvinchuk A P, Valakh M Y, Kruszynska M, Kolny-Olesiak J, Himcinschi C and Zahn D R T 2014 Raman scattering in orthorhombic $CuInS_2$ nanocrystals *phys. stat. sol. a* **211** 195–9

[40] Yeryukov N A, Milekhin A G, Sveshnikova L L, Duda T A, Pokrovsky L D, Gutakovskii A K, Batsanov S A, Rodyakina E E, Latyshev A V. and Zahn D R T 2014 Synthesis and Characterization of Cu_xS (x = 1–2) Nanocrystals Formed by the Langmuir–Blodgett Technique *J. Phys. Chem. C* **118** 23409–14

[41] Morante J R, Scheer R and Calvet W 2001 Raman scattering structural evaluation of CuInS2 thin films *Thin Solid Films* **387** 216–8

[42] Gasanly N M, Magomedov A Z, Melnik N N and Salamov B G 1993 Raman and Infrared Studies of AgIn5S8 and CuIn5S8 Single Crystals *Phys. status solidi* **177** K31–5

[43] Jeong S, Yoon H C, Han N S, Oh J H, Park S M, Min B K, Do Y R and Song J K 2017 Band-Gap States of AgIn 5 S 8 and ZnS − AgIn 5 S 8 Nanoparticles *J . Chem. Phys. C* **121** 3149−3155

[44] Azimi H, Kuhri S, Stahl M S, Hou Y, Guldi D M and Brabec C J 2015 Elucidating the Excited-State Properties of CuInS2 Nanocrystals upon Phase Transformation : Quasi -Quantum Dots Versus Bulk Behavior *Adv. Electron. Mater.* **1** 1500040

[45] Chen W, Qi J, Dong C, Chen J, Shen Z, He Y, Yang S, Chen T, Chen C, Li Y, Li M and Wang M 2019 Solution-Processed in Situ Growth of CuInS 2 Nanoparticle Films for Efficient Planar Heterojunction Solar Cells with a Dual Nature of Charge Generation *ACS Appl. Energy Mater.* **2** 5231–42

[46] Lee D and Kim J 2010 Characterization of sprayed CuInS 2 fi lms by XRD and Raman spectroscopy measurements *Thin Solid Films* **518** 6537–41

[47] Pe A, Morante J R and Scheer R 2000

MicroRaman scattering from polycrystalline CuInS 2 films : structural analysis *Thin Solid Films* **362** 208–12

[48] Chen B, Zhong H, Zhang W, Tan Z, Li Y, Yu C, Zhai T, Bando Y, Yang S and Zou B 2012 Highly emissive and color-tunable CuInS 2-based colloidal semiconductor nanocrystals: Off-stoichiometry effects and improved electroluminescence performance *Adv. Funct. Mater.* **22** 2081–8

[49] Papadimitriou D, Esser N and Xue C 2005 Structural properties of chalcopyrite thin films studied by Raman spectroscopy *phys. stat. sol.* **2643** 2633–43

[50] Lei S, Wang C, Liu L, Guo D, Wang C, Tang Q, Cheng B, Xiao Y and Zhou L 2013 Spinel Indium Sulfide Precursor for the Phase-Selective Synthesis of Cu − In − S Nanocrystals with Zinc-Blende, Wurtzite, and Spinel Structures *Chem. Mater.* **25** 2991–7

[51] Hong S P, Park H K, Oh J H, Yang H and Do Y R 2012 Comparisons of the structural and optical properties of o-AgInS2, t-AgInS2, and c-AgIn5S8 nanocrystals and their solid-solution nanocrystals with ZnS *J. Mater. Chem.* **22** 18939

[52] Koschel W, Sorger F and Baars J 1975 Optical phonons in I-III-VI2 compounds *J. Phys.* **36** 177–81

[53] Courtel F M and Hammami A 2010 Synthesis of n-type CuInS 2 Particles Using N -methylimidazole , Characterization and Growth Mechanism *Chem. Mater.* **48** 3752–61

[54] Courtel F M, Paynter R W, Marsan B and Morin M 2009 Synthesis, Characterization, and Growth Mechanism of n-Type CuInS2 Colloidal Particles *Chem. Mater.* **21** 3752–61

[55] Saucedo E, Izquierdo-roca V, Fontane X, Jaime-ferrer J S, Jacobo A and Ramon J 2011 Process monitoring of chalcopyrite photovoltaic technologies by Raman spectroscopy : an application to low cost electrodeposition based processes *New J. Chem.* **35** 453–60

[56] Alvarez-García J, Rudigier E, Rega N, Barcones B, Scheer R, Pérez-Rodríguez A, Romano-Rodríguez A and Morante J R 2003 Growth process monitoring and crystalline quality assessment of $CuInS(Se)_2$ based solar cells by Raman spectroscopy *Thin Solid Films* **431**–**432** 122–5

[57] Cabot A, Shavel A, Saucedo E, Bermudez V, Morante J R and Pe A 2011 Assessment of absorber composition and nanocrystalline phases in CuInS 2 based photovoltaic technologies by ex-situ / in-situ resonant Raman scattering measurements *Sol. Energy Mater. Sol. Cells* **95** S83–8

[58] Morell G, Katiyar R S, Weisz S Z, Walter T, Schock H W and Balberg I 2011 Crystalline phases at the p- to n- type transition in Cu-ternary semiconducting films *Appl. Phys. Lett.* **69** 987

[59] Oja I, Nanu M, Katerski A, Krunks M, Mere A, Raudoja J and Goossens A 2005 Crystal quality studies of CuInS2 films prepared by spray pyrolysis *Thin Solid Films* **480**–**481** 82–6

[60] Kusch P, Lange H, Artemyev M and Thomsen C 2011 Size-dependence of the anharmonicities in the vibrational potential of colloidal CdSe nanocrystals *Solid State Commun.* **151** 67–70

[61] Bhar G C 1978 Sphaleritelike vibration mode in chalcopyrites *Phys. Rev. B* **18** 1790–3

[62] Ohrendorf F W and Haeuseler H 1999 Lattice Dynamics of Chalcopyrite Type Compounds . Part I . Vibrational Frequencies *Cryst. Res. Technol.* **34** 339–49

[63] Camus C, Rudigier E, Abou-Ras D, Allsop N A, Unold T, Tomm Y, Schorr S, Gledhill S E, Köhler T, Klaer J, Lux-Steiner M C and Fischer C-H 2008 Phonon confinement and strain in $CuInS_2$ *Appl. Phys. Lett.* **92** 101922

[64] Dzhagan V M, Valakh M Y, Himcinschi C, Milekhin A G, Solonenko D, Yeryukov N A, Raevskaya O E, Stroyuk O L and Zahn D R T 2014 Raman and Infrared

Phonon Spectra of Ultrasmall Colloidal CdS Nanoparticles *J. Phys. Chem. C* **118** 19492–7

[65] Guc M, Litvinchuk A P, Guc M, Litvinchuk A P, Levcenko S, Valakh M Y, Bodnar I V., Dzhagan V M, Izquierdo-Roca V, Arushanov E, Perez-Rodrıguez A and Pérez-Rodríguez A 2016 Optical phonons in the wurtzstannite Cu2ZnGeS4 semiconductor: Polarized Raman spectroscopy and first-principle calculations *RSC Adv.* **6** 13278–85

[66] Oliva F, Kretzschmar S, Colombara D, Tombolato S, Maria C, Redinger A, Saucedo E, Broussillou C, Goislard T, Monsabert D, Unold T, Dale P J, Izquierdo-roca V and Pérez-rodríguez A 2016 Optical methodology for process monitoring of chalcopyrite photovoltaic technologies : Application to low cost Cu (In , Ga)(S , Se) 2 electrodeposition based processes *Sol. Energy Mater. Sol. Cells* **158** 168–83

[67] Dzhagan V, Valakh M, Mel'nik N, Rayevska O, Lokteva I, Kolny-Olesiak J and Zahn D R T 2012 Phonon Spectra of Small Colloidal II-VI Semiconductor Nanocrystals *Int. J. Spectrosc.* **2012** 532385-1–6

[68] Neto E S F, da Silva S W, Morais P C, Vasilevskiy M I, Pereira-da-Silva M A and Dantas N O 2011 Resonant Raman scattering in CdS_xSe_{1-x} nanocrystals: effects of phonon confinement, composition, and elastic strain *J. Raman Spectrosc.* **42** 1660–9

[69] Lange H, Artemyev M, Woggon U and Thomsen C 2009 Geometry dependence of the phonon modes in CdSe nanorods *Nanotechnology* **20** 045705

[70] Lin C, Gong K, Kelley D F and Kelley A M 2015 Size-Dependent Exciton–Phonon Coupling in CdSe Nanocrystals through Resonance Raman Excitation Profile Analysis *J. Phys. Chem. C* **119** 7491–8

[71] Kobosko S M and Kamat P V. 2018 Indium-Rich AgInS2-ZnS Quantum Dots - Ag-/Zn-Dependent Photophysics and Photovoltaics *J. Phys. Chem. C* **122** 14336–44

[72] Susaki M, Yamamoto N, Prevot B and Schwab2 C 1996 Multiple-Phonon Resonant Raman Scattering in CuGaS2 *Jpn. J. Appl. Phys.* **35** 1652–6

[73] Lange H, Artemyev M, Woggon U, Niermann T and Thomsen C 2008 Experimental investigation of exciton-LO-phonon couplings in CdSe/ZnS core/shell nanorods *Phys. Rev. B* **77** 193303

[74] Valakh M Y, Litvinchuk A P, Pekar G S and Polysskii G N 1981 Multiple-Phonon Resonant Raman Scattering in Zn<inf>1–x</inf> Cd<inf>x</inf>Se Crystals *Phys. status solidi* **104**

[75] Kelley A M 2013 Resonance Raman overtone intensities and electron-phonon coupling strengths in semiconductor nanocrystals. *J. Phys. Chem. A* **117** 6143−6149

[76] Lin C, Kelley D F, Rico M and Kelley A M 2014 The "surface optical" phonon in CdSe nanocrystals *ACS Nano* **8** 3928–38

[77] Gasanly N M, El-Hamid S A, Gasanova L G and Magomedov A Z 1992 Vibrational Spectra of Spinel-Type Compound CuIn5S8 *Phys. Status Solidi* **169** K115–8

[78] Gasanly N M 2016 Infrared-active modes in Ag 3 Ga 5 S 9 and Ag 3 In 5 S 9 single crystals : An influence of trivalent cation substitution *Optik (Stuttg).* **127** 6858–61

[79] Bodnar I V, Karoza A G, Kudritskaya E A and Smirnova A G 1997 Vibrational spectra of In2S3, CuInsS8 and AgInsS8 compounds with a spinel structure *J. Appl. Spectrosc.* **64** 263–5

[80] Neumann H, Kissinger W, Sobotta H, Riede V, Tomlinson R D and Avgerinos N 1984 Infrared study of the lattice vibrations in CuInS2 *Czech. J. Phys. B* **34** 69–77

[81] Sinha M M, Ashdhir P, Gupta H C and Tripathi B B 1995 Vibrational Analysis of Zone Centre Phonons in Sulfospinels AgIn5S8 and CuIn5S8 *phys. stat. sol.* **33** K33–6

[82] Gasanly N M 2016 Optical constants of silver and copper indium ternary sulfides

from infrared reflectivity measurements *Infrared Phys. Technol.* **75** 168–72

[83] Reiss P, Protière M and Li L 2009 Core/shell semiconductor nanocrystals *Small* **5** 154–68

[84] Nanocrystals C, Berends A C, Stam W Van Der, Hofmann J P, Bladt E, Meeldijk J D, Bals S and Donega C D M 2018 Interplay between Surface Chemistry, Precursor Reactivity, and Temperature Determines Outcome of ZnS Shelling Reactions on CuInS 2 Nanocrystals *Chem. Mater.* **30** 2400–13

[85] Milekhin A, Sveshnikova L, Duda T, Surovtsev N, Adichtchev S, Ding L and Zahn D R T 2010 Vibrational spectra of quantum dots formed by Langmuir–Blodgett technique *J. Vac. Sci. Technol. B Microelectron. Nanom. Struct.* **28** C5E22

[86] Azhniuk Y M, Milekhin A G, Gomonnai A V., Hutych Y I, Lopushansky V V. and Zahn D R T 2009 Phonon spectra of quaternary $Cd_{1-y}Zn_yS_{1-x}Se_x$ semiconductor nanocrystals grown in a glass matrix *phys. stat. sol. c* **6** 2068–71

[87] Milekhin A G, Yeryukov N A, Sveshnikova L L, Duda T A, Himcinschi C, Zenkevich E I and Zahn D R T 2012 Resonant Raman scattering of ZnS, ZnO, and ZnS/ZnO core/shell quantum dots *Appl. Phys. A* **107** 275–8